Materials Science & Engineering A 705 (2017) 105–113

Contents lists available at ScienceDirect

Materials Science & Engineering A

journal homepage: www.elsevier.com/locate/msea

Microstructures and mechanical behavior of aluminum-copper lap joints

Xianglong Zhou[a], Gang Zhang[a], Yu Shi[a,*], Ming Zhu[a], Fuqian Yang[b,*]

[a] State key Laboratory of Advanced Processing and Recycling Non-ferrous Metals, Lanzhou University of Technology, Lanzhou 730050, PR China
[b] Department of Chemical and Materials Engineering, University of Kentucky, Lexington 40506, USA

ARTICLE INFO

Keywords:
Al-Cu joint
Microstructure
Intermetallic compound
Shear strength
Brittle fracture

ABSTRACT

5052 aluminum alloy and pure copper (T2) are joined, using a low heat input pulsed double-electrode gas metal arc welding (DE-GMAW)-brazing method with $AlSi_{12}$ filler metal. The effects of welding current (heat input) on the microstructure and mechanical behavior of the joints, which consist of Al-Al welding zone and Al-Cu brazing zone, are investigated. The Al-Cu welding zone mainly consists of α-Al solid solution and Al-Cu eutectic phase in coral-like shape. There exists a layer of Al_2Cu intermetallic compound (IMC) in the Al-Cu brazing zone. Using the theory of thermal activation process, a quadratic relation between the thickness of the IMC layer and welding current intensity is derived. The experimental result supports this relationship. The shear strength of the Al-Cu joints first increases with the increase of the welding current (heat input), reaches a maximum of 17.66 MPa, and then decreases with the increase of the welding current due to the dispersion of the Al_2Cu IMCs of large sizes in the Al alloy. Fracture of the Al-Cu lap joints occurs at three different positions, and the corresponding failure mechanisms are discussed according to the morphologies of fracture surfaces.

1. Introduction

Aluminum-copper (Al-Cu) dissimilar joints are desirable as structural components in a variety of mechanical structures used in chemical, metallurgical, and electronic devices and systems. The Al-Cu joints likely possess high electrical and heat conductivities, and good corrosion resistance due to the use of both Al and Cu [1–3]. However, joining Al with Cu faces many challenges because of great differences in physical properties (thermal conductivity, thermal expansion coefficient, and melting point) between Al and Cu, and the formation of brittle intermetallic compounds (IMCs) which can deteriorate the mechanical responses of dissimilar joints [4–6].

Various solid-state welding methods have been developed to join dissimilar metals, such as friction stir welding (FSW), explosion welding, and ultrasonic spot welding. Tan et al. [7] used FSW to form butt joints from 5A02 Al alloy and copper, and observed the presence of nanophases, including Al_4Cu_9, Al_2Cu_3 and Al_2Cu around the Al/Cu interface. Tensile strength of the butt joints reached ~ 130 MPa. Henryk et al. [8] studied the microstructure and phase constitution near the interface of Al-Cu joints prepared by the explosion welding, and found the IMCs of Cu_9Al_4, CuAl and $CuAl_2$ which seriously deteriorated the tensile strength of the joints. Using ultrasonic spot welding and Al2219 alloy particles as an interlayer, Ni et al. [9] joined Al alloy with Cu. Their results suggest that the process parameters play an important role in determining the tensile-shear strength of the joints, and fracture occurred in the base metal of Cu.

Recently, cold metal transfer (CMT) technique developed from gas metal arc welding with low heat input has been used to join Al/Cu dissimilar metals. Cai et al. [10] used CMT to join AA6061-T6 Al alloy to Cu, and observed a large amount of brittle IMCs near the interface between the weld metal and the base metal. Feng et al. [11] prepared lap joints from 1060 Al sheet and Cu from CMT, and studied the effects of heat input on the interface morphology, microstructure, and joint strength. The maximum load that an Al-Cu lap joint can sustain was ~ 0.983 kN for the lap joint prepared with the welding parameters of 102 A and 25 mm/s. There is little study focusing on the Al-Cu joints prepared by low heat input pulsed double-electrode gas metal arc welding (DE-GMAW)-brazing methods.

It is known that the IMCs formed in the Al-Cu joints significantly determine the mechanical behavior and durability of the joints, and are dependent on the heat input during joining and the composition of the filler materials. Precise control of the heat input will likely determine the quality of the dissimilar joints with given filler materials. In this study, a pulsed DE-GMAW, which can control the heat input, was used to join an Al alloy sheet to a Cu sheet with ER4047 filler wire. The effects of the welding current (heat input) on the microstructures and shear strength of the Al-Cu joints were studied. The facture surfaces were also analyzed.

* Corresponding authors.
E-mail addresses: shiyu@lut.cn (Y. Shi), fyang2@uky.edu (F. Yang).

http://dx.doi.org/10.1016/j.msea.2017.08.056
Received 27 May 2017; Received in revised form 14 August 2017; Accepted 16 August 2017
Available online 18 August 2017

Table 1
Chemical compositions of 5052 Al alloy and filler wire (wt%).

Material	Si	Mg	Fe	Cu	Zn	Mn	Cr	Al
5052 Al-alloy	0.25	2.2–2.8	0.40	0.10	0.10	0.10	0.15–0.35	Bal.
ER4047	12.00	0.10	0.80	0.30	0.20	0.15	–	Bal.

2. Experimental details

2.1. Materials

5052 Al alloy of 1 mm in thickness and commercial Cu (T2) of 2 mm in thickness were used. The filler metal was ER4047 Al wire of 1.2 mm in diameter. Tables 1 and 2 list the chemical compositions of the 5052 Al alloy, ER4047 Al wire, and Cu. Prior to joining, the surfaces of 5052 Al alloy sheets were brushed by a stainless steel brush to remove surface oxides, and then cleaned by acetone. The Cu sheets were cleaned with acetone.

2.2. Joining

The pulsed DE-GMAW is an arc welding method modified from gas metal arc welding (GMAW) and gas tungsten arc welding (GTAW). The following briefly describes the pulsed DE-GMAW method. A GTAW torch is inserted between the GMAW torch and the work-piece to decouple a welding current (I_{bypass}) from total current (I_{total}), which reduces the current (I_{main}) flowing into the base metal, i.e. $I_{main} = I_{total} - I_{bypass}$. This result allows precise control of the heat input into the base metal by regulating the bypass current, and stable metal transfer is achieved with low heat input to the work-piece. However, using the bypass torch cannot completely meet the requirement for the joining of Al/Cu dissimilar metals, which requires further reduction of the heat input. To further reduce the heat input, pulsed currents are used for both the bypass current and the main current. With synchronous control of the current waveforms of the main and bypass currents, low heat input into the base metal is achieved precisely, and the droplet is transferred from the wire tip to the weld pool at a lower current than that needed for the spray transfer of metal in normal GMAW process. For detailed information of the experimental setup, see the work by Shi et al. [12]. Note that the pulsed DE-GMAW has been successfully used in the joining of Al/steel [13–15].

Fig. 1a shows a schematic configuration of the lap joint, which was formed from 150 × 50 mm sheets. The 5052 Al alloy sheet was placed on top of the Cu sheet in a lap configuration with an overlap distance of 10 mm. The angle between the two torches was ~ 45°, and the filler wire was fed with an angle of 60° to the normal of the specimen surface. During welding, argon gas was used as shielding gas to prevent oxidation of the welded surfaces, and the flow rates of argon gas were 20 and 5 L/min for the main and bypass loops, respectively. The welding speed was 0.5 m/min, and the pulse duty-ratio and frequency were 20% and 80 Hz for both the main and bypass closed loops, respectively.

2.3. Single-lap shear test

Fig. 1b shows the geometrical dimensions of the single-lap specimens. Shear tests were performed on a tensile machine at room temperature to measure the interface strength of the Al-Cu joints. Displacement control was used with a constant crosshead speed of 0.5 mm/min.

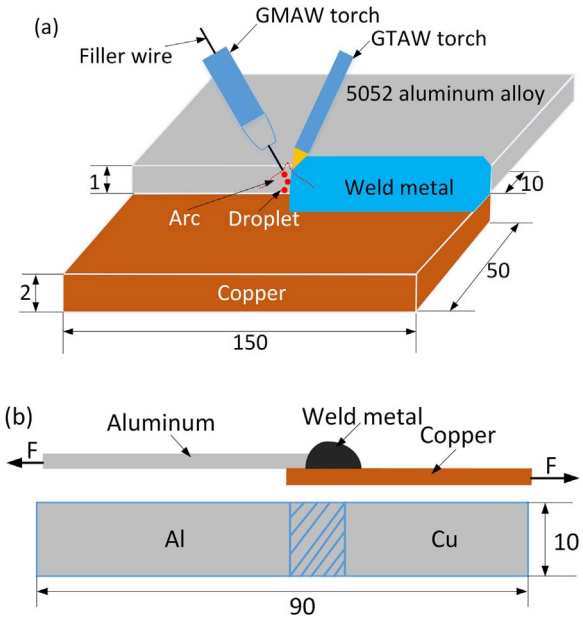

Fig. 1. (a) Schematic diagram of the joining of an Al/Cu lap joint, and (b) geometrical configuration of a shear specimen (unit: mm).

The shear strength of a joint, $\sigma_{t\text{-}s}$, was calculated from the following equation

$$\sigma_{t-s} = \frac{F}{l \cdot \delta} \quad (1)$$

where F is the maximum load at which local cracking occurs, l is the width of the specimen (10 mm), and δ is the length of the Al alloy plate jointed to the copper plate and can be measured from the cross-section of the lap joint shown in Fig. 2. The results reported are the average values of three tests of the same conditions.

2.4. Materials characterization

The cross-section of the joints was mechanically ground and polished to obtain mirror-like surface following the standard metallographic procedure. The macrostructures and microstructures of the joints were observed and analyzed by optical microscopy (OM) and scanning electron microscope (SEM) equipped with a backscattered electron detector. The element distributions in the joints were analyzed using energy dispersive spectrometer (EDS). The crystal structure of the joints was analyzed with Cu K*a* radiation line on an X-ray diffractometer with patterns recorded in a range of 10–90°.

3. Results and discussion

3.1. Microstructures of Al-Cu lap joints

Fig. 2 shows the topology and cross-section of the Al-Cu lap joints prepared with several welding currents. For small welding current through the main loop, there is no enough heat input into the base metal of Cu, and Al droplet cannot spread well on the Cu surface due to poor wetting. Poor and non-uniform weld beads, as shown in Fig. 2a, were formed. Increasing the welding current into the base metal of Cu

Table 2
Chemical composition of commercial Cu (T2) (wt%).

Element	Cu + Ag	Fe	Pb	Ni	Sb	S	As	Bi	Other
wt%	≥ 99.9	≤ 0.005	≤ 0.005	≤ 0.005	≤ 0.002	≤ 0.005	≤ 0.002	≤ 0.001	0.06

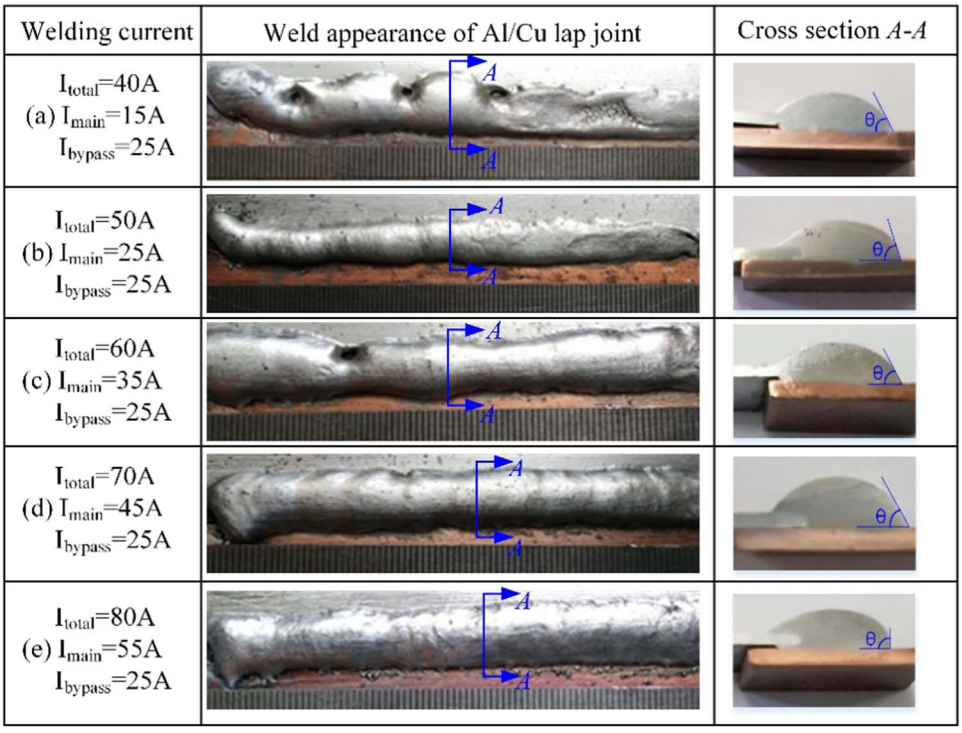

Fig. 2. Topology and cross-section of the Al-Cu joints made with several welding currents.

leads to the decrease of the width of the weld beads and the slight increase in the height of the weld beads due to the improvement of the wetting and spreading of Al droplet on the Cu surface, as shown in Fig. 2b-e. Such a result is due to the decrease of the surface tension and viscosity of Al droplet with the increase of the heat input. However, large welding current (heat input) can cause damage to the base metal of Cu, introducing welding defects, such as undercuts and cracks shown in Fig. 2d and e. Also, increasing welding current (heat input) can cause the formation of brittle Al-Cu IMCs through the dissolution of Cu in Al alloy, which can weaken the Al-Cu joints.

Fig. 3 shows SEM images of an Al-Cu lap joint prepared with the parameters of I_{main} = 55 A and I_{bypass} = 25 A. It is evident that there exist three zones; (I) Al alloy-weld metal fusion zone, (II) weld metal zone, and (III) Cu-weld metal brazing interface zone. The SEM image of Fig. 3b reveals the microstructure of the Al-weld metal fusion zone (zone I) and the fusion line denoted by a red solid line. There are columnar grains distributed near the fusion line, which grew towards the weld metal since the molten Al alloy solidifies in the direction with the maximum negative-temperature gradient from base metal into the center of the weld pool [16].

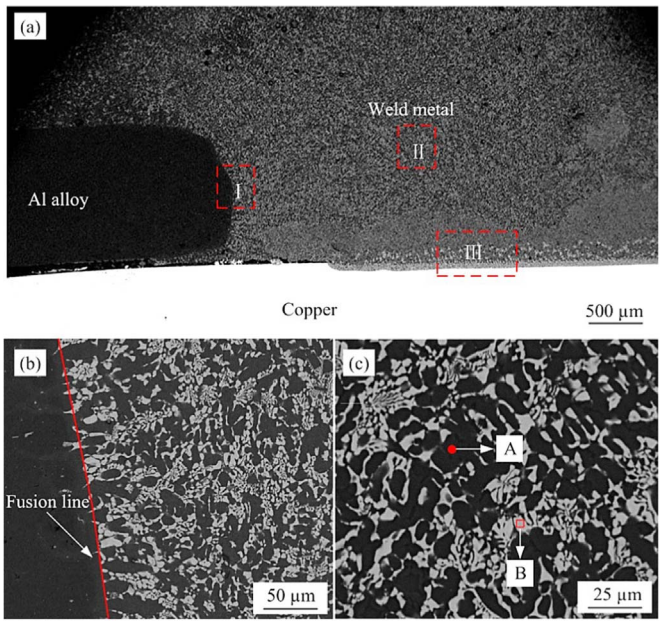

Fig. 3. SEM images of an Al-Cu lap joint (I_{main} = 55 A, I_{bypass} = 25 A); (a) cross-section view, (b) enlarged view of zone I, and (c) enlarged view of zone II.

EDS analysis was performed on the zone II of the Al-Cu joint. Table 3 lists the chemical compositions of the areas of A and B shown in Fig. 3c. According to the results listed in Table 3, one can conclude that the weld metal mainly consists of α-Al solid solution, as denoted by A, and Al-Cu eutectic alloy in coral-like shape, as denoted by B.

Fig. 4 shows the SEM images of the Cu-weld metal brazing interface zones (zone III shown in Fig. 3a) formed with different main currents. The interfacial zone can be divided into three regions: (II) corresponding to Al alloy-weld metal, (IV) corresponding to the layer of Al-Cu IMCs, and (V) corresponding eutectic Al-Cu. During the welding-brazing, the Cu atoms on the Cu surface dissolve and migrate/diffuse to the molten Al alloy (region II) associated with the heat transfer and convection in the molten metal. The migration/diffusion of Cu into the molten Al alloy leads to the formation of a layer of Al-Cu IMCs. The thickness of the Al-Cu IMCs is dependent on local temperature and the flow of the molten metal, and is limited by the rapid cooling of the weld metal [11]. Using the Al-Cu and Al-Si phase diagrams [17,18] and the EDS analysis, the structures in the regions of C and D in Fig. 4e were found to consist of Si and Al_2Cu, respectively, which are listed in Table 3. There are Al_2Cu IMCs of large sizes and Si precipitates in the Al alloy matrix. This result suggests the formation of a layer of Al_2Cu IMCs

Table 3
Chemical composition of denoted zones.

Points	Al	Cu	Si	Possible phase
A	92	2.2	5.8	α(Al) + eutectic Al-Si
B	74.5	24.2	1.3	eutectic Al-Cu
C	1.1	1.2	97.7	Si
D	66.3	33.2	0.5	Al_2Cu

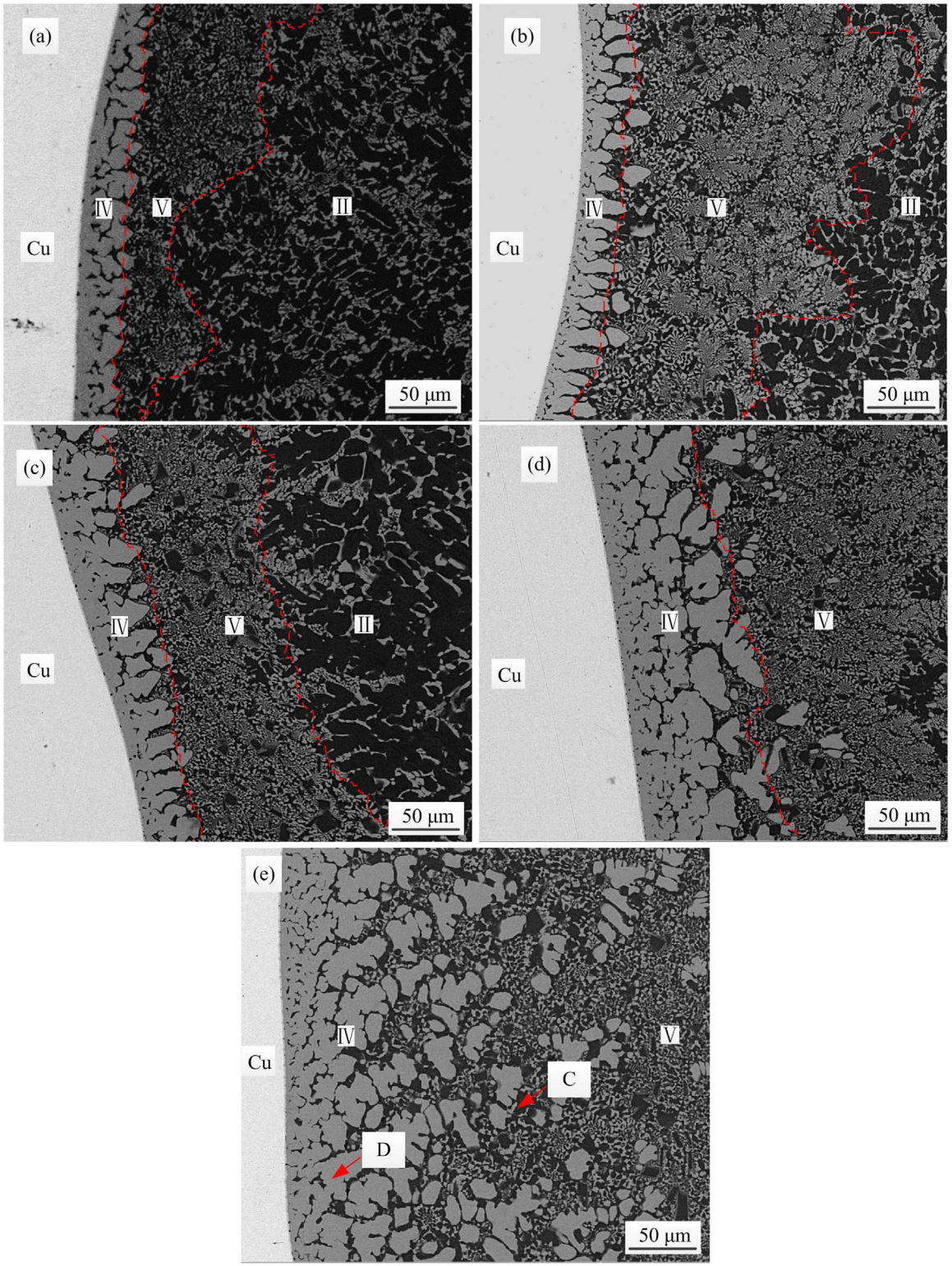

Fig. 4. SEM images of the Cu-weld metal brazing interface zones formed with different main currents (I_{bypass} = 25 A); (a) I_{main} = 15 A, (b) I_{main} = 25 A, (c) I_{main} = 35 A, (d) I_{main} = 45 A, and (e) I_{main} = 55 A.

in the Cu-weld metal brazing interface zone.

3.2. Intermetallic compound layer

From the SEM images shown in Fig. 4a-e, one can note that the surface of the IMC layer on the Cu side is presented in relatively uniform and flat shape, and the surface of the IMC layer on the side of the weld metal is presented in zigzag shape. The Al_2Cu IMCs grew into the weld metal in the form of coarse columnar structures. The larger the current, the higher is the mobility of Cu in the Al alloy. Increasing the welding current into the base metal of Cu leads to the formation of Al_2Cu IMCs of large sizes, which disperse in the Al alloy, as supported in Fig. 4d and e.

Fig. 5 shows the variation of the thickness of the Al_2Cu IMC layer

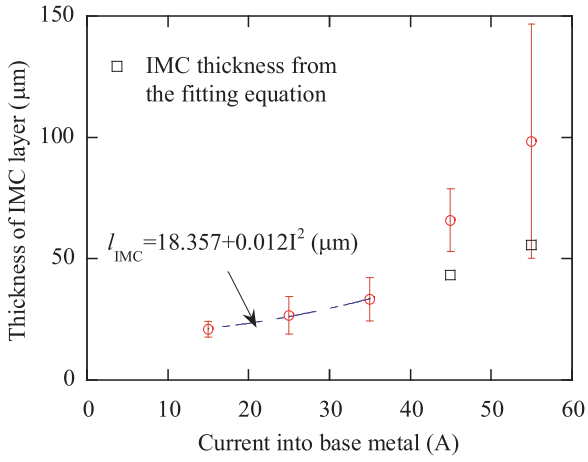

Fig. 5. Variation of the thickness of the Al_2Cu IMC layer with the welding current into the base metal of Cu.

with the welding current into the base metal of Cu. It is evident that average thickness of the Al_2Cu IMC layer increases with the increase of the welding current into the base metal of Cu. Such behavior reveals the effect of the welding current on the growth of the Al_2Cu IMC layer. It is known that the growth rate of an IMC layer is determined by temperature and driving force, which can be expressed as

$$\frac{dl_{IMC}}{dt} = \alpha e^{-Q/RT} \tag{2}$$

where l_{IMC} is the average thickness of an IMC layer, t is time, α is a proportionality constant associated with the driving force, Q is the activation energy for the rate process, R is the gas constant, and T is absolute temperature. The welding current has two possible contributions to the growth of the Al_2Cu IMC layer; one is Joule heat, resulting in the increase of temperature, and the other is the driving force associated with electron wind force. The temperature increase due to the passage of a welding current of I through the base metal of Cu can be calculated as

$$\Delta T = \beta I^2 \tag{3}$$

with β being a constant proportional to the resistance in the main loop. Assume that the effect of electron wind force on the proportionality constant of α can be expressed as

$$\alpha = \alpha_0 + \chi I \tag{4}$$

with α_0 being the proportionality constant without welding current, and χ being a constant associated with the field-assisted motion of Cu atoms.

Substituting Eqs. (3) and (4) into Eq. (2) yields

$$\frac{dl_{IMC}}{dt} = (\alpha_0 + \chi I)e^{-Q/R(T_0+\beta I^2)} \tag{5}$$

where T_0 is the temperature of the base metal of Cu associated with the growth of the Al_2Cu IMC layer with $I = 0$. For $T_0 >> \beta I^2$, Eq. (5) can be simplified to the order of I^2 as

$$\frac{dl_{IMC}}{dt} \approx (\alpha_0 + \chi I)\exp\left[-\frac{Q}{RT_0}(1 - \frac{\beta I^2}{T_0})\right] = a + bI + cI^2 + O(I^3) \tag{6}$$

which gives

$$l_{IMC} \approx a' + b'I + c'I^2 \tag{7}$$

i.e. the thickness of the Al_2Cu IMC layer is a quadratic function of the welding current into the base metal of Cu for the same welding time. Here, a, b, c, a', b', and c' are constants. Note that the linear term in Eq. (7) represents the contribution of electron wind force.

Assume that the contribution of electron wind force is negligible for $I \leq 35$ A. Using Eq. (7) to curve-fit the data in Fig. 5, one obtains

$$l_{IMC} \approx 18.357 + 0.012I^2 \tag{8}$$

in the unit of micrometer. For the comparison, the fitting results are also included in Fig. 5. It is evident that the results from Eq. (8) are the same as the experimental data, validating the assumption that the effect of electron wind on the growth of the Al_2Cu IMC layer is negligible. Using Eq. (8), the IMC thicknesses solely controlled by the thermal-assisted migration for $I = 45$ and 55 A are calculated and represented by the square symbol in Fig. 5. The experimental results for $I = 45$ and 55 A are larger than the results calculated from Eq. (8).

In principle, one can calculate the IMC thickness as

$$l_{IMC} = l_{thermal} + l_{EW} \tag{9}$$

in which the $l_{thermal}$ is the IMC thickness controlled by the thermal-assisted migration and l_{EW} is the IMC thickness controlled by electron wind. Subtracting $l_{thermal}$ calculated from Eq. (8) from l_{IMC} for $I = 35$, 45, and 55 A, one obtains of l_{EW} of 0, 22.6, and 42.9 μm, respectively. It is evident that there exists a linear relationship between I and l_{EW}, in accord with the linear term in Eq. (7). Thus, the contribution of electron wind to the IMC growth is not negligible for $I \geq 35$ A.

3.3. Mechanical behavior of the Al-Cu lap joints

Microhardness test was performed over the Al-Cu lap joints along the HD (horizontal direction) and VD (vertical direction) directions, shown schematically in Fig. 6a, using Vickers indenter. The maximum normal load was 0.5 N, and the loading time was 10 s Fig. 6b and c show the spatial distribution of the Vickers hardness. Note that the Vickers hardness reported is an average of three tests from three different specimens prepared with the same welding parameters. It is evident that the Vickers hardness of the weld metal is always larger than the base metals of Al alloy and Cu. From Fig. 6c, one can note that the Vickers hardness increases from the weld metal zone (region II) to Al-Cu eutectic zone (region V), to the IMC layer, and then decrease to the base metal of Al alloy. Such behavior suggests the diffusion of Si to the region, in which eutectic reaction occurs. The higher the concentration of Si, the larger is the Vickers hardness. The Al_2Cu IMCs have the largest Vickers hardness of ~ 370 HV, as shown in Fig. 6c. Note that the Vickers hardness of the Al_2Cu IMCs layer is larger than 272 HV for Al_2Cu IMCs and less than 444 HV for AlCu IMCs reported by Aravind et al. [19]. Such a difference likely is due to the effect of Al and Cu matrixes. The structures reported by Aravind et al. [19] consisted of ribbon-like Al_2Cu IMCs, which was supported by Al(Cu) matrix. There likely exists significant substrate effect on the hardness measurement of the Al_2Cu IMCs. In contrast to the ribbon-like Al_2Cu IMCs reported by Aravind et al. [19], the Al_2Cu IMCs formed during the pulsed DE-GMAW processing were presented in a relatively dense structure, as shown in Fig. 4. There is little or limited substrate effect on the hardness measurement of the Al_2Cu IMCs, and the Vickers hardness of the Al_2Cu IMCs with a relatively dense structure is expected to be larger than that with the substrate effect. It needs to point out that the Al_2Cu IMCs are brittle and reduce the ductility of the Al-Cu joints.

Fig. 7 shows the variation of the shear strength of the Al-Cu joints with the welding current into the base metal of Cu. The shear strength of the Al-Cu joints increases first with the increase of the welding current into the base metal of Cu to the maximum of ~ 17.66 MPa, and then decreases with the increase of the welding current. Such a difference is likely due to the formation of the Al_2Cu IMCs and the difference in the stress state. For the tensile of a single lap joint, the joint experiences both shear and bending deformation since there is misalignment between the base metals. The bending deformation can activate local defects, such as voids, around the interfaces between the base metals and the weld metal, which reduce the strength of the lap joints under concurrent loading of shear and bending. Also, the presence of the Al_2Cu IMCs of large sizes in the Al alloy will introduce local

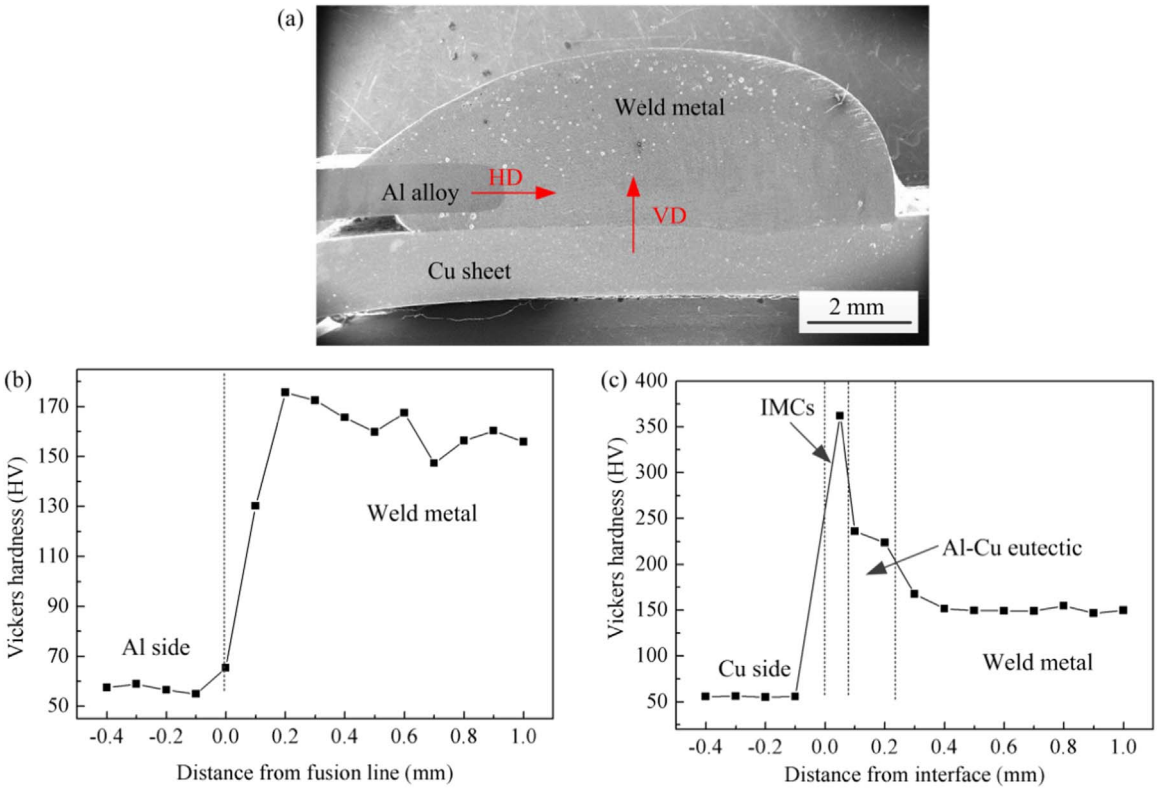

Fig. 6. (a) Schematic diagram of the directions for the hardness measurement; spatial distribution of Vickers hardness over an Al-Cu lap joint (I_{bypass} = 25 A, I_{main} = 55 A): (b) along horizontal direction (HD), and (c) along vertical direction (VD).

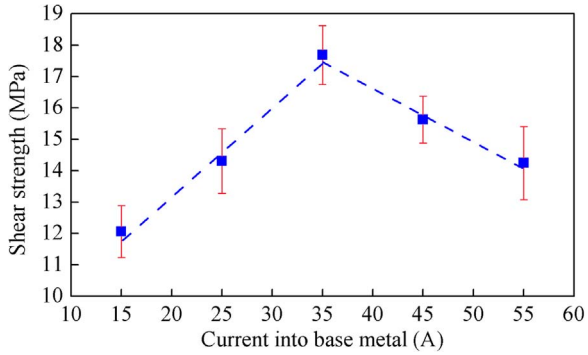

Fig. 7. Variation of the shear strength of the Al-Cu joints with the welding current into the base metal of Cu.

stress concentration, which accelerates the failure of the lap joints when local stress is large enough to introduce local delamination or cracking. This trend leads to the decrease of the shear strength for the thickness of the Al_2Cu IMCs layer larger than or equal to 33.16 μm, corresponding to the welding current into the base metal of Cu being larger than or equal to 35 A.

It is interesting to note that the shear strength of the Al-Cu lap joints increases with the increase of the welding current into the Cu base metal for the current less than or equal to 35 A, which corresponds to the increase of the thickness of the Al_2Cu IMCs layer to 33.16 μm. From Fig. 4, one can note that there is no observable difference among the morphologies of the Al_2Cu IMCs layer, and the thickness of the Al_2Cu IMCs layer increases with the increase of the current into the Cu base metal. This result suggests that a relatively uniform layer of Al_2Cu IMCs indeed enhances the strength of the Al-Cu lap joints.

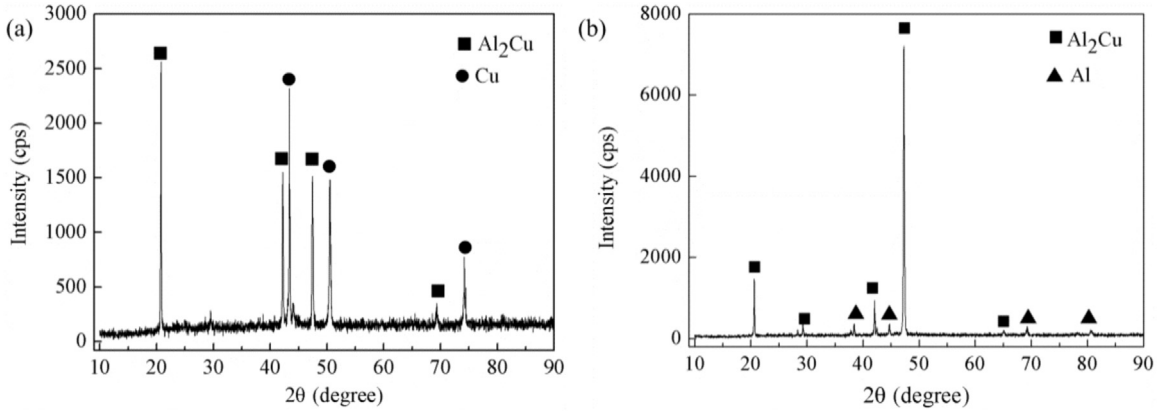

Fig. 8. XRD pattern of a fractured surface (I_{main} = 55 A, I_{bypass} = 25 A); (a) near the interface between the base metal of Cu and the Al_2Cu IMCs layer, and (b) near the interface between the Al alloy and the Al_2Cu IMCs layer.

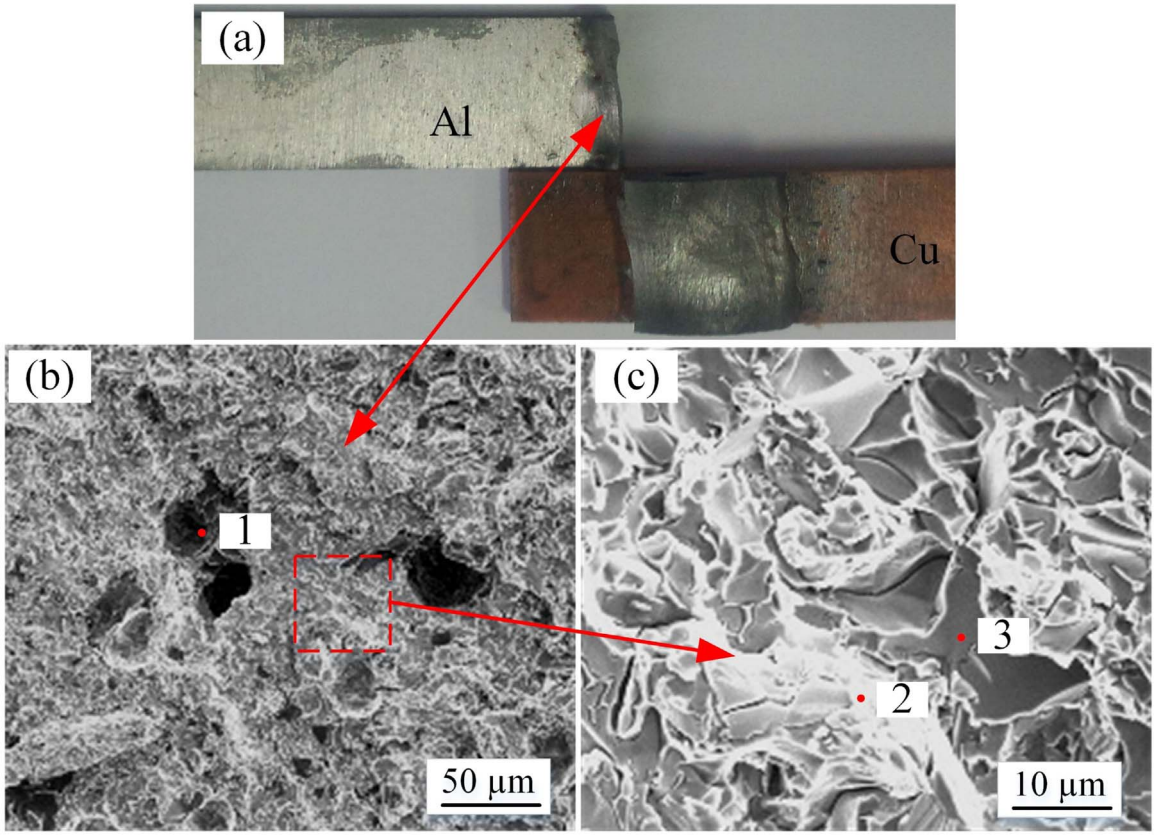

Fig. 9. Fracture surfaces of an Al-Cu joint around the fusion line (I_{main} = 25 A, I_{bypass} = 25 A); (a) optical micrograph, (b) SEM image, and (c) enlarged view of the fracture surface.

3.4. Analysis of fracture behavior

XRD was used to analyze the microstructures of the Al-Cu lap joints. Fig. 8 shows the XRD patterns near the interface between the base metal of Cu and the Al_2Cu IMCs layer and that between the Al alloy and the Al_2Cu IMCs layer. Both XRD patterns reveal the presence of the Al_2Cu IMCs in accord with the SEM images shown in Fig. 4. Note that no peaks associated with Si are present since there is little amount of Si in the Al alloy.

Figs. 9–11 show SEM images of the fracture surfaces of the Al-Cu lap joints. In general, fracture occurred at three different positions in the Al-Cu lap joints subjected to tensile loading. Some Al-Cu lap joints failed either around the fusion line (Fig. 9) or in the heat affected zone (HAZ) (Fig. 10), and most Al-Cu lap joints failed around the welding-brazing interface zone (Fig. 11). The phase composition of fracture surfaces, which is listed in Table 4, also identified by EDS.

According to the SEM images, one can note that the position of the fracture surface varies with the welding current into the base metal of Cu (heat input). For the current of 25 A into the base metal of Cu, the lap joint failed along the fusion line (Fig. 9), around which the main constituents are eutectic Al-Cu and eutectic Al–Si, as supported by the EDS results (Table 4). The Al alloy near the fusion line melted, and the microstructures coarsened with the condition of a large welding current (heat input). From Fig. 6, one can note that the Vickers hardness of the IMCs layer is the largest, and the Vickers hardness near the fusion line is ~ 52HV, suggesting that the area around the fusion line has a lower strength in comparison with the strength of the Al alloy. The region around the fusion line is the weakest area of the Al-Cu lap joints. Also, some dimples are observed from Fig. 9b, which might be associated with the fracture of the lap joint under tensile loading.

According to Fig. 9, no local structural instability (necking) is observable, suggesting quasi-brittle fracture although there are some dimples presented on the fracture surface. The river pattern again confirms the brittle feature of the fracture.

With the welding current into the base metal being increased to 45 A, the lap joints failed around the HAZ, as shown in Fig. 10. This results is due to the formation of large amount of IMCs and Al-Si, Al-Cu eutectics in the Al-Cu brazing zone and in the weld metal near the fusion line zone. Both the IMCs and the eutectics increase local strength. Generally, there is little change in the microstructures of the HAZ of the Al alloy, and the HAZ has the lowest strength. Hence, the HAZ becomes the weakest region of the lap joints under the current conditions. Note that there are dimples formed over the fracture surface shown in Fig. 10b, suggesting the ductile characteristic of the fracture in accord with the structural instability (necking) appearing near the fracture. The fracture surface is presented in a cup-cone shape.

With the welding current into the base metal being increased to 55 A, the lap joint ruptured at the welding-brazing interface between the weld metal and the base metal of Cu, as shown in Fig. 11a. Intercrystalline cracks are observed on the fracture surface (Fig. 11b), suggesting the characteristic of brittle fracture. There are Si precipitates on the fractured surface as represented by the material at the spot 6 in the enlarged view of Fig. 11c. The Si precipitates and Al_2Cu IMCs reduce the bonding strength between the weld metal and the base metal of Cu and make it easy to cause local separation and crack propagation.

4. Conclusions

Joining Al with Cu is of practical importance in chemical, metallurgical, and electronic devices and systems. Using the pulsed DE-GMAW-brazing technique, the plate of 5052 Al alloy was joined with the plate of commercially copper (T2). The microstructures and mechanical behavior of the Al-Cu lap joints were investigated. Some conclusions can be drawn as follows.

1. Using the pulsed DE-GMAW-brazing technique, we can precisely

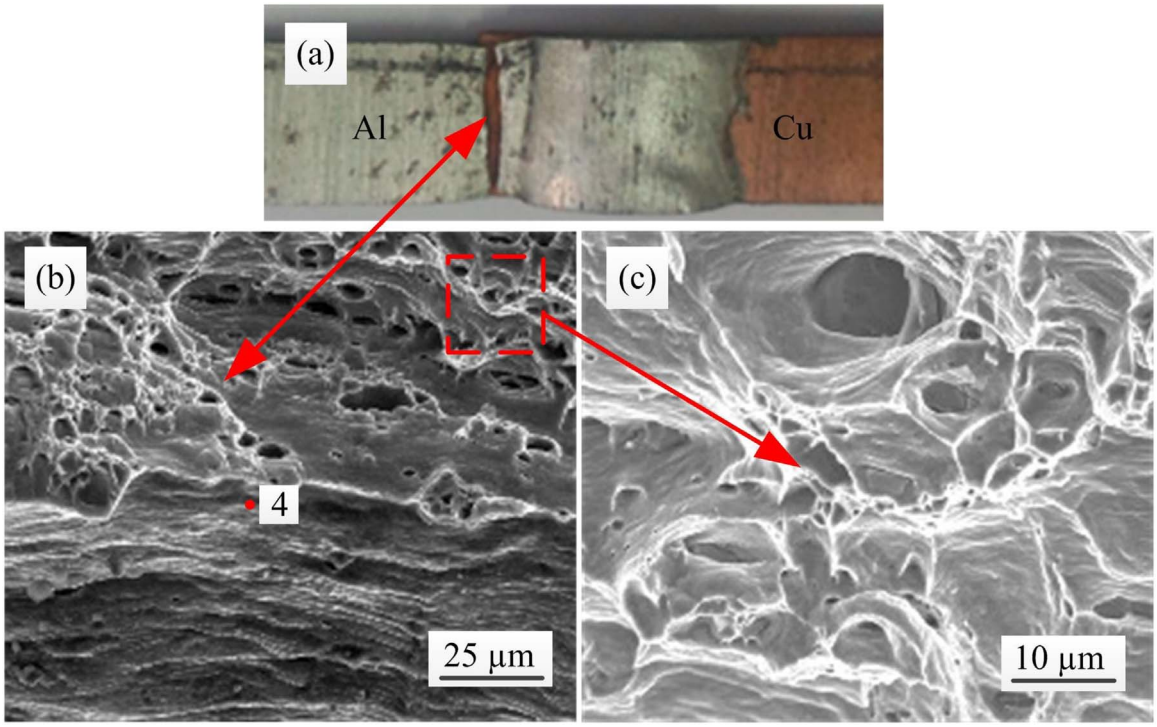

Fig. 10. Fracture surfaces of an Al-Cu joint in the heat affected zone (I_{main} = 45 A, I_{bypass} = 25 A); (a) optical micrograph, (b) SEM image, and (c) enlarged view of the fracture surface.

control the heat input into the base metal of Cu, which allows us to control the formation of the IMCs and the microstructures of the lap joints.

2. There exist three different zones in the Al-Cu lap joints; fusion zone between the Al alloy and the weld metal, the weld metal zone and the brazed interface zone between the Cu and the weld metal. The brazed zone mainly consists of Al_2Cu IMCs and eutectic Al-Cu. The thickness of the Al_2Cu IMCs layer increase with the increase of the welding current (heat input) into the Cu base metal.
3. Using the theory of thermal activation process, a quadratic relation

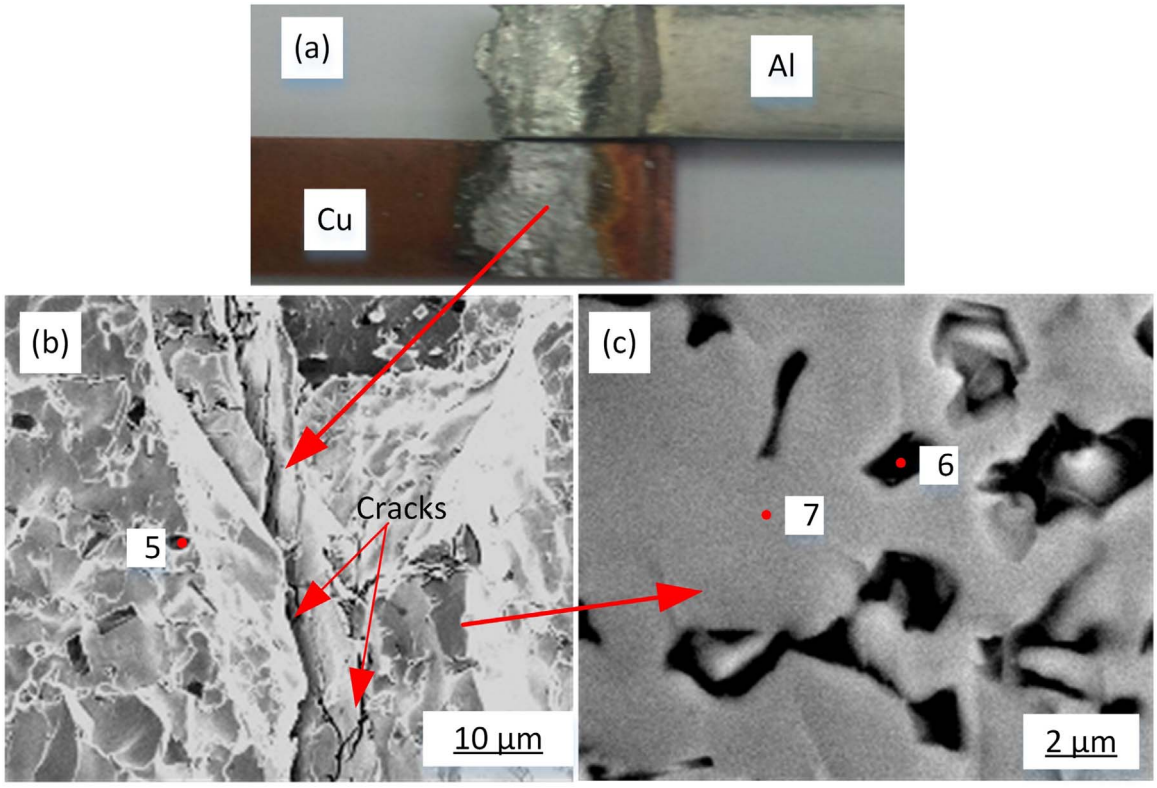

Fig. 11. Fracture surfaces of an Al-Cu joint around the welding-brazing interface zone (I_{main} = 55 A, I_{bypass} = 25 A); (a) optical micrograph, (b) SEM image, and (c) enlarged view of the fracture surface.

Table 4
Chemical compositions of selected spots on the fracture surfaces (at%).

Spot	Al	Cu	Si	Possible phase
1	68.3	2.1	29.6	Al–Si eutectic
2	68.1	30.2	1.7	Al-Cu eutectic
3	58.2	24.7	17.2	Al–Cu, Al–Si eutectic
4	100	…	…	Al
5	3.7	4.6	91.7	Si
6	66.8	32.7	0.5	Al_2Cu
7	32.2	16.4	51.4	Si + Al_2Cu

between the thickness of the IMC layer and welding current intensity is derived. The experimental results support this relationship and suggest that the electron wind force has negligible effect on the growth of the Al_2Cu IMCs layer for $I \leq 35$ A.

4. The shear strength of the Al-Cu lap joints increases with the increase of welding current into the base metal of Cu, reaches the maximum at the welding current of 35 A, and then decreases with the increase of the welding current duo to the dispersion of the Al_2Cu IMCs of large sizes in the Al alloy. For the relatively uniform Al_2Cu IMCs layer, the shear strength of the Al-Cu lap joints increases with the increase of the thickness of the Al_2Cu IMCs layer, corresponding to the welding current being less than or equal to 35 A.
5. The fracture surface varies with the welding current into the base metal of Cu (heat input), which is controlled by the microstructures formed during the pulsed DE-GMAW-brazing.

Acknowledgment

This work was supported by the National Natural Science Foundation of China (#51675256), the Hong Liu Outstanding Talent Training Plan of Lanzhou University of Technology (#J201201), Natural Science Foundation of Gansu Province (#145RJZA119) and the Open Foundation of State Key Laboratory of Advanced Processing and Recycling of Non-ferrous Metals (SKLAB 0201400802014008).

References

[1] H. Dong, W. Hu, Y. Duan, X. Wang, C. Dong, Dissimilar metal joining of aluminum alloy to galvanized steel with Al–Si, Al–Cu, Al–Si–Cu and Zn–Al filler wires, J. Mater. Process. Technol. 212 (2012) 458–464.
[2] P. Xue, D.R. Ni, D. Wang, B.L. Xiao, Z.Y. Ma, Effect of friction stir welding parameters on the microstructure and mechanical properties of the dissimilar Al-Cu joints, Mater. Sci. Eng. A 528 (2011) 4683–4689.
[3] A.S. Zoeram, S.H.M. Anijdan, H.R. Jafarian, T. Bhattacharjee, Welding parameters analysis and microstructural evolution of dissimilar joints in Al/Bronze processed by friction stir welding and their effect on engineering tensile behavior, Mater. Sci. Eng. A 687 (2017) 288–297.
[4] M. Weigl, F. Albert, M. Schmidt, Enhancing the ductility of laser-welded copper-aluminum connections by using adapted filler materials, Phys. Procedia 12 (2011) 332–338.
[5] W.F. Xu, J.H. Liu, D.L. Chen, Material flow and core/multi-shell structures in a friction stir welded aluminum alloy with embedded copper markers, J. Alloy Compd. 509 (2011) 8449–8454.
[6] P. Kah, C. Vimalraj, J. Martikainen, R. Suoranta, Factors influencing Al-Cu weld properties by intermetallic compound formation, Int. J. Mech. Eng. 10 (2015) 1–13.
[7] C.W. Tan, Z.G. Jiang, L.Q. Li, Y.B. Chen, X.Y. Chen, Microstructural evolution and mechanical properties of dissimilar Al–Cu joints produced by friction stir welding, Mater. Des. 51 (2013) 466–473.
[8] P. Henryk, L.D. Lidia, P. Mariusz, Microstructure and phase constitution near the interface of explosively welded aluminum/copper plates, Metall. Mater. Trans. A 44 (2013) 3836–3851.
[9] Z.L. Ni, F.X. Ye, Weldability and mechanical properties of ultrasonic joining of aluminum to copper alloy with an interlayer, Mater. Lett. 182 (2016) 19–22.
[10] Z.P. Cai, B.Q. Ai, R. Cao, Q. Lin, J.H. Chen, Microstructure and properties of aluminum AA6061-T6 to copper (Cu)-T2 joints by cold metal transfer joining technology, J. Mater. Res. 31 (2016) 2876–2887.
[11] J. Feng, Y. Liu, Q. Sun, L. Wu, Microstructures and properties of aluminum-copper lap-welded joints by cold metal transfer technology, Adv. Eng. Mater. 17 (2015) 1480–1485.
[12] Y. Shi, G. Zhang, Y. Huang, L. Lu, Pulsed double electrode GMAW-brazing for joining of aluminum to steel, Weld. J. 93 (2014) 216s–224s.
[13] Y. Shi, L. Shao, J. Huang, Y. Gu, Effects of Si and Mg elements on the microstructure of aluminum-steel joints produced by pulsed DE-GMA welding-brazing, Mater. Sci. Technol. 29 (2013) 1118–1124.
[14] Y. Shi, J. Li, G. Zhang, J. Huang, Y. Gu, Corrosion behavior of aluminum-steel weld-brazing joint, J. Mater. Eng. Perform. 25 (2016) 1916–1923.
[15] J. Huang, X. He, Y. Guo, Z. Zhang, Y. Shi, D. Fan, Joining of aluminum alloys to galvanized mild steel by the pulsed DE-GMAW with the alternation of droplet transfer, J. Manuf. Process. 25 (2017) 16–25.
[16] K. Sindo, Welding Metallurgy, Wiley, Hoboken, 2003.
[17] N. Ponweiser, C.L. Lengauer, K.W. Richter, Re-investigation of phase equilibria in the system Al–Cu and structural analysis of the high-temperature phase $\eta 1 - Al1 - \delta Cu$, Intermetallics 19 (2011) 1737–1746.
[18] J.L. Murray, A.J. McAlister, The Al-Si (aluminum-silicon) system, J. Phase Equilib. 5 (1984) 74–84.
[19] M. Aravind, P. Yu, M.Y. Yau, D.H.L. Ng, Formation of Al_2Cu and AlCu intermetallics in Al(Cu) alloy matrix composites by reaction sintering, Mater. Sci. Eng. A 380 (2004) 384–393.